Satellite spectra of the $K\alpha$ resonance line of heliumlike nickel, Ni XXVII, from tokamak-fusion-test reactor plasmas: Comparison between theory and experiment

M. Bitter, H. Hsuan, V. Decaux,* B. Grek, K. W. Hill, R. Hulse,
L. A. Kruegel,† D. Johnson, S. von Goeler, and M. Zarnstorff
Plasma Physics Laboratory, Princeton University, P.O. Box 451, Princeton, New Jersey 08543
(Received 1 April 1991; revised manuscript received 1 July 1991)

Satellite spectra of the $K\alpha$ line of heliumlike nickel, Ni XXVII, recorded from tokamak-fusion-test reactor (TFTR) Ohmic plasmas with well-defined experimental conditions and central electron temperatures in the range 2–5 keV, have been compared with theoretical predictions. The relevant plasma parameters that determine the spectral features, i.e., the electron and ion temperatures, and the relative abundances of Ni XXV, Ni XXVI, and Ni XXVII have been obtained from least-squares fits of synthetic spectra to the experimental data. Both the dielectronic satellites and the satellites which are produced by collisional inner-shell excitation are well described by the theory given by Bombarda *et al.* [Phys. Rev. A **37**, 504 (1988)] and Vainshtein and Safronova (unpublished). The electron-temperature results derived from the fits are in good agreement with electron-temperature measurements from independent diagnostics. However, the values obtained for the relative abundances of Ni XXV, Ni XXVI, and Ni XXVII are larger by factors of 1.3–2 compared to recent coronal-equilibrium predictions of Zastrow, Källne, and Summers [Phys. Rev. A **41**, 1427 (1990)]. Plasma-modeling calculations performed with the multi-ion-species-transport [R. A. Hulse, Nucl. Technol. Fusion **3**, 259 (1983)] code show that these deviations can be explained by radial ion transport assuming for the ion-transport diffusion coefficient D values in the range 1–2.5 $m^2 s^{-1}$. However, the observed deviations may be partially ascribed to theoretical uncertainties of the ionization and recombination rate coefficients used for the coronal-equilibrium calculations. Systematic discrepancies are found to exist between the predicted and observed intensity ratios, x/w, y/w, and z/w, of the heliumlike lines w, $1s^2\,{}^1S_0-1s2p\,{}^1P_1$; x, $1s^2\,{}^1S_0-1s2p\,{}^3P_2$; y, $1s^2\,{}^1S_0-1s2p\,{}^3P_1$; and z, $1s^2\,{}^1S_0-1s2s\,{}^3S_1$.

I. INTRODUCTION

In a previous paper [1], we presented a spectrum of the $K\alpha$ line of heliumlike nickel, Ni XXVII, and its associated satellites, and compared these experimental data with theoretical predictions from Hartree-Fock-Slater calculations [2,3] and the Z-expansion method [4,5]. The spectrum had been observed from the plasma of a single tokamak-fusion-test reactor (TFTR) discharge with a central electron temperature of 4 keV using a high-resolution ($\lambda/\Delta\lambda=18\,000$) Johann curved-crystal spectrometer. The spectrometer permitted simultaneous observation of spectral features in the wavelength range 1.585 to 1.610 Å. This wavelength range includes the heliumlike lines $1s^2\,{}^1S_1-1s2p\,{}^1P_1$ (w), $1s^2\,{}^1S_1-1s2p\,{}^3P_{1,2}$ (x,y), and $1s^2\,{}^1S_1-1s2s\,{}^3S_1$ (z) of Ni XXVII and the associated lithiumlike and berylliumlike satellites due to transitions $1s^2nl-1s2pnl'$ and $1s^22snl-1s2p2snl'$ with $n\geq 2$ in Ni XXVI and Ni XXV. (The letters w, x, y, and z correspond to Gabriel's notation [6].) In Ref. [1], emphasis was placed on the identification of the spectral components and a comparison of the experimental and theoretically predicted wavelengths for the heliumlike lines and the satellites with main quantum numbers $n=2-4$. The experimental wavelengths of these spectral features were determined relative to the position of the resonance line w, to which we assigned the theoretical wavelength value. The observed and predicted relative wavelengths were found to be in agreement to within 0.2 mÅ. On the other hand, the relative abundances of Ni XXVI, Ni XXV, and Ni XXVII inferred from the observed satellite-to-resonance-line ratios were substantially larger than the predicted coronal-equilibrium values [7].

Further experimental data on the satellite spectrum of Ni XXVII obtained from the Joint European Torus (JET) were published in two subsequent papers by Bombarda *et al.* [8] and Zastrow, Källne, and Summers [9]. Bombarda *et al.* [8] presented a spectrum for the extended wavelength range 1.584 to 1.621 Å, which also includes the boronlike satellites from transitions in Ni XXIV. This spectrum was constructed by juxtaposition of five spectra (each covering a wavelength range of 10 mÅ). The spectra had been recorded from a number of very similar Ohmic discharges with central electron temperatures of 3 keV. The measurements were performed with different settings of a Johann spectrometer which had a spectral resolution of $\lambda/\Delta\lambda=20\,000$. Reference 8 also provided a more complete set of theoretical data for satellites with $n\leq 7$ (and extrapolated data for the $n\geq 8$ satellites) from calculations using the SUPERSTRUCTURE code [10,11] as well as data on rate coefficients for the different processes of line excitation. The excitation processes considered for the heliumlike lines w, x, y, and z included (a) direct electron impact excitation, (b) electron impact excitation of states with $n>2$ followed by cascades, (c) excitation by recombination of hydrogenlike nickel, Ni XXVIII, and (d) excitation of the line z by inner-shell ionization of lithi-

umlike nickel, Ni XXVI. The experimental results reported by Bombarda *et al.* [8] were similar to those described in Ref. 1: The observed and predicted relative wavelength were in agreement to within 0.2 mÅ. However, the relative abundances of Ni XXIV, Ni XXV, Ni XXVI, and Ni XXVII were found to be larger than coronal equilibrium values (see Ref. 29 in Ref. [8]) by approximately factors of 2. For the spectrum discussed in Ref. 8, the observed relative intensities of the heliumlike lines w, x, y, and z appeared to be in good agreement with the theoretical predictions.

In the more recent paper [9], Zastrow, Källne, and Summers presented results from an analysis of a large number ($\sim$3000) of Ni XXVII spectra from JET tokamak plasmas and investigated the satellite-to-resonance-line ratios as a function of the electron temperature. These spectra had been observed with the "standard setting" of the JET spectrometer used for ion temperature measurements. The spectra, therefore, covered only the limited wavelength range 1.5840 to 1.5965 Å. This wavelength range includes the heliumlike lines w and x, the lithiumlike ($n \geq 3$) dielectronic satellites of w, and the lithiumlike $1s^2 2s\ ^2S_{1/2} - 1s2s2p\ ^2P_{1/2}$ satellite (t). The satellite t is excited partially by dielectronic recombination of Ni XXVII and partially by inner-shell excitation of Ni XXVI. The data analyzed by Zastrow, Källne, and Summers were obtained from a variety of JET discharges with different experimental conditions, which included discharges with Ohmic heating, auxiliary-ion cyclotron heating and neutral-beam injection. The electron temperature results derived from the relative intensities of the dielectronic $n \geq 3$ satellites and the resonance line w were found to be in good agreement with electron temperature measurements from the electron cyclotron emission and laser Thomson scattering. However, the major conclusions of Ref. [9] are in contrast to the earlier results reported in Ref. [8]. In particular, Zastrow, Källne, and Summers conclude that the relative abundances of Ni XXVI and Ni XXVII (which were derived from the intensity ratio t/w) are in good agreement with the more recent coronal-equilibrium calculations used in Ref. 9. On the other hand, they find that the observed intensity ratio of the heliumlike lines x/w is significantly larger than the theoretical predictions for the entire investigated range of electron temperatures, 2 to 12 keV. Discrepancies between predicted and observed intensity ratios, x/w, y/w, and z/w for the heliumlike lines of Ti XXI have been reported previously [12].

The intensity ratios of the heliumlike lines have important diagnostic applications for measurements of the electron density [13] in solar flares [14,15] and in laser-produced high-density plasmas of inertial-confinement experiments; they are also used for measurements of nonthermal-electron velocity distributions [16–18] in tokamak plasmas with auxiliary electron-cyclotron heating. The fact that the theoretical predictions for these intensity ratios are in disagreement with results from tokamak experiments (JET and TFTR) is a matter of concern. The electron densities in tokamak plasmas are well below the critical densities for which the electron-collision rates are comparable with the radiative decay rates of the $1s2p$ states of Ti XXI and Ni XXVII [6]. Therefore, one should expect that the intensity ratios of these heliumlike lines are in agreement with theoretical predictions [19–23], if they are observed from tokamak plasmas with thermal-electron velocity distributions.

In this paper, we present a quantitative comparison of the observed and predicted relative intensities of the spectral lines in the extended wavelength range 1.585 to 1.615 Å as a function of the electron temperature. The spectra have been observed from a series of 50 Ohmically heated TFTR discharges with well-defined experimental conditions and central electron temperatures in the range 2 to 5 keV. As described in Ref. [1], the measurements were performed with a Johann spectrometer, which permits simultaneous observation of the entire spectral range. The relevant plasma parameters, such as the ion and electron temperatures, T_i and T_e, and the relative abundances, $n_{\text{Ni XXVI}}/n_{\text{Ni XXVII}}$ and $n_{\text{Ni XXV}}/n_{\text{Ni XXVII}}$, have been determined from least-squares fits of synthetic spectra to the experimental data, and the obtained parameter values were then compared with results from independent diagnostics. The synthetic spectra were constructed from the theoretical data given in Refs. [8] and [24]. Due to the use of least-squares-fit methods in our analysis, it is possible to determine these parameters very accurately and to quantify (with error bars) the discrepancies between the observed and the theoretical spectra.

The paper is organized as follows: In Sec. II, we describe the experimental conditions and the experimental arrangement. In Sec. III, we discuss the data analysis. Section IV presents the obtained results for (a) the electron temperature, (b) the relative abundances of Ni XXV, Ni XXVI, and Ni XXVII, (c) the intensity ratios of the heliumlike triplet and singlet lines, and (e) the broadening and shift of the apparent resonance-line profile, which is caused by unresolved satellites. Conclusions are presented in Sec. V.

II. EXPERIMENTAL CONDITIONS

The experimental data were recorded from a series of 50 Ohmically heated TFTR discharges (shot numbers 29 720–29 770) with the TFTR horizontal crystal spectrometer [25]. This spectrometer permits the simultaneous observation of the Ni XXVII satellite features in the entire wavelength range 1.58 to 1.61 Å with a spectral resolution of $\lambda/\Delta\lambda = 7500$. The TFTR tokamak discharges were helium-prefill discharges, so-called "clean-up shots," which are normally used to remove the absorbed deuterium from the plasma limiter. Due to the reduced gas fueling from the limiter, the electron density decreased gradually for the series of these "clean-up shots." Correlated with the decrease of the electron density was an increase of the central electron temperature, which provided very suitable conditions for an investigation of line-intensity ratios as a function of the electron temperature. Since each of the discharges had an extended period (2 to 5 sec) of steady-state conditions, it was possible to record the spectral data with very small statistical errors. Excitation of the heliumlike lines by charge-exchange recombination of Ni XXVIII with neutral

deuterium atoms, which is an important mechanism in discharges with neutral-deuterium injection, is assumed to be negligible for these Ohmic discharges.

The discharge parameters were as follows: The major and minor plasma radii were $R=2.46$ m and $a=0.81$ m. The plasma current I_p and the toroidal magnetic field B_t were $I_p=1.4$ MA and $B_t=3.5$ T (for shots 29 720–29 745), and $I_p=1.8$ MA and $B_t=4.2$ T (for shots 29 748–29 770). The radial profiles of the electron temperature T_e and electron density n_e were nearly flat over the central region between $R=2.30$ m and $R=2.75$ m. Examples of data taken with the Thomson-scattering [26] system from two discharges, shots 29 726 and 29 766, chosen from the beginning and the end of the shot sequence, are presented in Figs. 1 and 2, and show the consistency of the radial-profile shapes for these experiments. The central plasma density decreased from 4.5 to 2.0×10^{19} m^{-3}, and the central electron temperature increased from 2 to 5 keV, as shown in Fig. 3. The steplike increase of the central electron density and temperature with shot 29 748 was caused by an increase of the plasma current and the magnetic field.

Survey spectra of the emitted x-ray radiation were recorded with the TFTR pulse height analysis (PHA) system [27], and are shown in Fig. 4. These spectra consist of a bremsstrahlung-and-recombination continuum and $K\alpha$-line radiation from metal impurity ions. The slope of the continuum spectrum is a measure of the electron temperature. The results obtained from the continuum spectra in Fig. 4(a) and 4(b) are in good general agreement with the central electron temperature from the Thomson-scattering diagnostic shown in Figs. 1 and 2. The observed intensity of each $K\alpha$ peak is a measure of the total concentration of the corresponding metal impurity. The energy resolution ($\sim$250 eV) of the PHA system is not sufficient to resolve the line spectra emitted from the different metal-ion charge states.

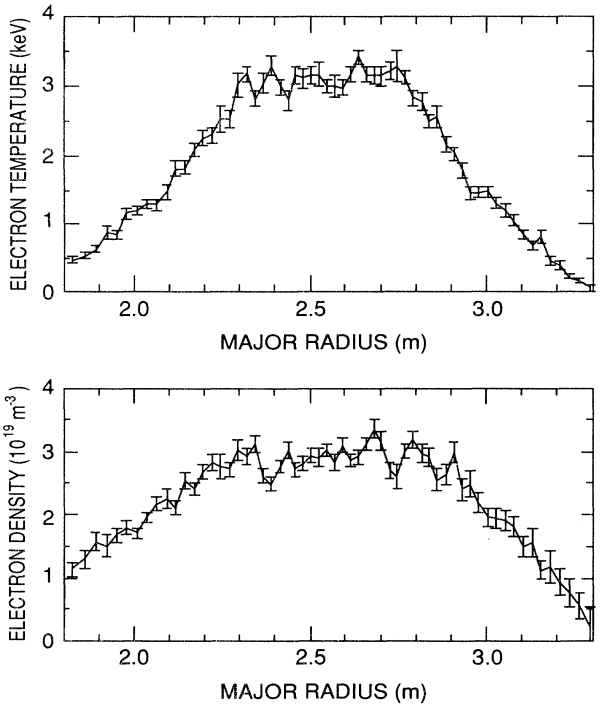

FIG. 1. Radial profiles of the electron temperature and electron density from TFTR shot 29 726 obtained from the Thomson-scattering diagnostic.

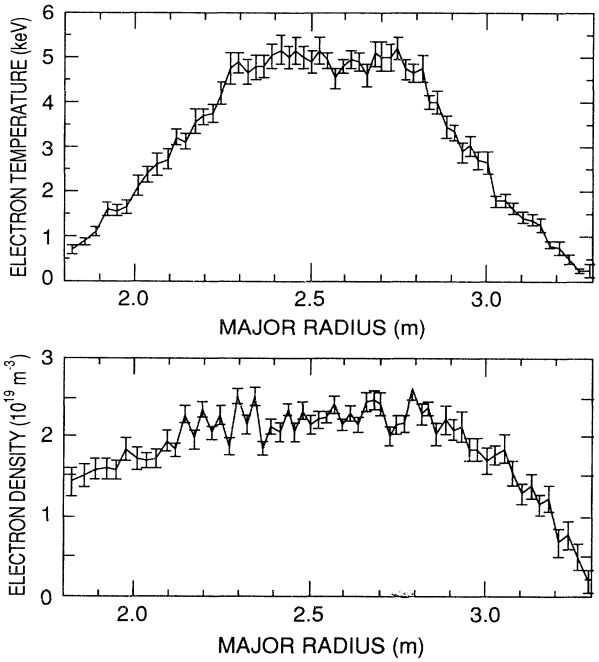

FIG. 2. Radial profiles of the electron temperature and electron density from TFTR shot 29 766 obtained from the Thomson-scattering diagnostic.

Resolved spectra of the Ni XXVII heliumlike lines and the associated satellites, as recorded with the TFTR horizontal crystal spectrometer, are shown in Fig. 5. The main spectral components have been identified using Gabriel's notation [6] and have been explained in Ref. [1]. The solid lines represent synthetic spectra constructed

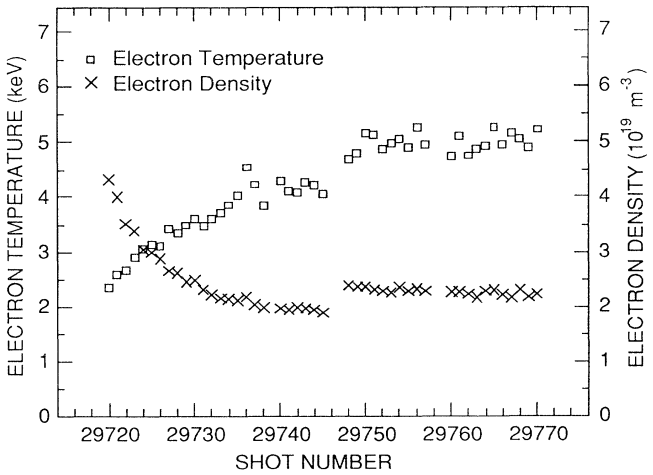

FIG. 3. Central electron temperature and central electron density for the investigated sequence of TFTR discharges.

from the theoretical data as described in detail in the following section. We note that the spectrum shown in Fig. 5(a) is almost identical to the spectrum presented in Ref. [8]. This spectrum will be discussed in more detail in Sec. IV B for comparison of our results with those given in Ref. [8].

III. DATA ANALYSIS

The analysis is based on a comparison of the experimental data with synthetic spectra of the theoretically predicted features, the intensities of which depend upon the electron temperature T_e and the relative abundances of Ni XXVIII, Ni XXVII, Ni XXVI, and Ni XXV [6,8]. These parameters have been determined from *least-squares fits* of the synthetic spectra to the experimental data.

Since the predominant part of the observed line radiation was emitted from the extended hot central region of the TFTR plasmas with nearly constant electron temperature (see Figs. 1 and 2), we assume that the observed intensity ratios can be *directly* compared to the ratios of the line emissivities predicted for the central electron-temperature values. In other words, we did not use chord integrals of the theoretical line emissivities along the sight line of the spectrometer for this comparison. A justification for this assumption is given in Sec. IV B. Due to this simplification, our analysis is not subject to the theoretical uncertainties inherent in model-dependent calculations of the radial ion-charge-state distribution, which is needed for the calculation of chord integrals.

The synthetic spectra are composed of approximately 100 spectral lines. Theoretical wavelengths for the heliumlike lines and for the $n=2$ satellites were taken from Vainshtein and Safronova [24]; theoretical wavelengths for the $n \geq 3$ satellites, line strengths $F_2(s)$ for the $n \geq 2$ satellites, and excitation rate coefficients were taken from Bombarda *et al.* [8]. The experimental spectrum was normalized to the theoretical wavelength value [24] of 1.5884 Å for the resonance line w. For this reason the wavelengths from Ref. [8] were increased by a constant amount of 2.8 Å.

The parameters T_e, T_i, and the relative abundances of Ni XXVII, Ni XXVI, and Ni XXV were determined from least-squares fits of the synthetic spectra to the experimental data according to the following procedure.

Step 1: A least-squares fit of the synthetic spectrum was performed to the spectral features in the wavelength range from 1.5850 to 1.5912 Å, which includes the resonance line w and the *dielectronic* satellites with $n \geq 3$. From this fit we obtained values for T_e and T_i. The value for T_e was kept constant for steps 2 through 4 of the fitting procedure. The value obtained for T_i was taken as the final value.

Step 2: The dielectronic contributions to the $n=2$ satellites, m, s, t, a, r, k, and j were constructed for the T_e value obtained in step 1 based on the theoretical predic-

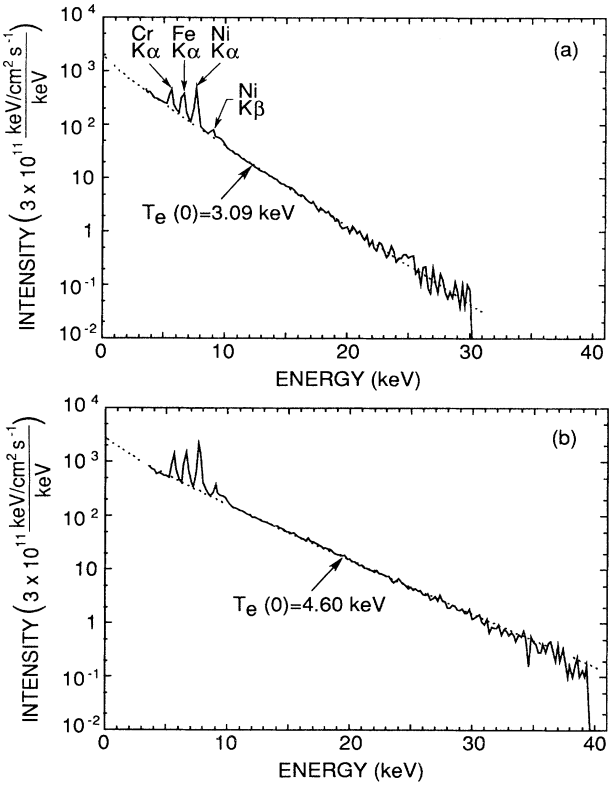

FIG. 4. Survey spectra of the soft-x-ray radiation as a function of photon energy recorded by the TFTR PHA system for (a) shot 29 726 and (b) shot 29 766. The data were accumulated during the period of steady-state conditions from 2 to 5 s.

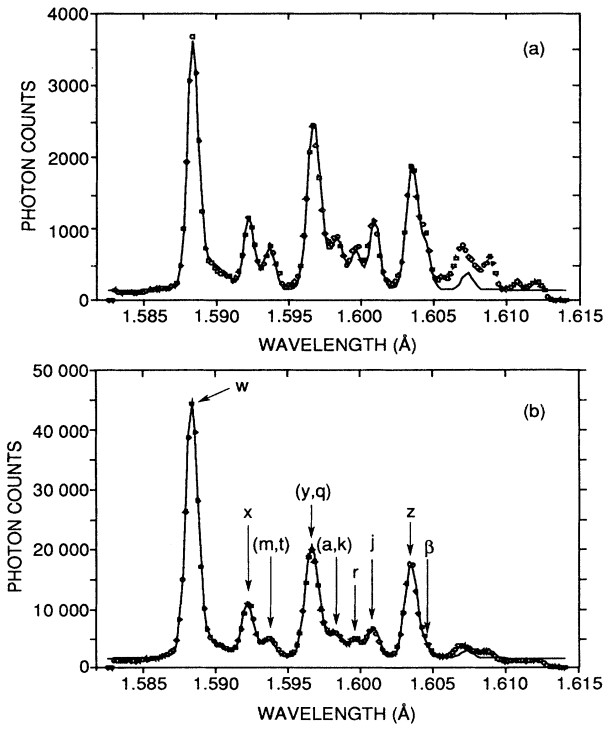

FIG. 5. Satellite spectra of the $K\alpha$ line of Ni XXVII recorded by the TFTR horizontal x-ray crystal spectrometer from (a) shot 29 726 and (b) shot 29 766. The solid lines represent least-squares fits of synthetic spectra to the experimental data.

tions for the relative intensities of these contributions with respect to the resonance line w.

Step 3: The relative abundances $n_{\text{Ni XXVI}}/n_{\text{Ni XXVII}}$ and $n_{\text{Ni XXV}}/n_{\text{Ni XXVII}}$ were determined from a fit of satellites q, r, s, t, and β in the wavelength range 1.5850 to 1.6053 Å. These satellites are predicted to be partially or entirely produced by collisional inner-shell excitation.

Step 4: The relative intensities of the intercombination and forbidden lines (x, y, and z) and the resonance line w were determined. The intensity ratios x/w, y/w, and z/w were expressed in terms of "enhancement factors" that compared the observed intensity ratios with those predicted for the processes of electron-impact excitation (including cascades).

Step 5: The final values for the parameters T_e, $n_{\text{Ni XXVI}}/n_{\text{Ni XXVII}}$ and $n_{\text{Ni XXV}}/n_{\text{Ni XXVII}}$, and the "enhancement factors" for the intensity ratios of the heliumlike lines were obtained from a least-squares fit to the data in the entire spectral range, 1.5850 to 1.6053 Å.

IV. RESULTS

Performing the analysis as described in the previous section, we found that each of the observed spectra could be well approximated by a synthetic spectrum. An important general result is that only three parameters, T_e, $n_{\text{Ni XXVI}}/n_{\text{Ni XXVII}}$, and $n_{\text{Ni XXV}}/n_{\text{NI XXVII}}$, were needed to reproduce the observed satellites features. In general, the initial electron-temperature values, obtained from the fit of the $n \geq 3$ dielectronic satellites in step 1, already described well the intensities of the strong $n=2$ dielectronic satellites. Indeed, the differences between the initial and the final T_e values obtained in step 5 were typically less than 0.3 keV. Moreover, the values obtained for $n_{\text{Ni XXVI}}/n_{\text{Ni XXVII}}$ and $n_{\text{Ni XXV}}/n_{\text{Ni XXVII}}$ from the least-squares fits in step 3 yielded an excellent representation not only of the satellites q and β, which are predicted to be entirely produced by collisional inner-shell excitation from the $n_{\text{Ni XXVI}}$ and $n_{\text{Ni XXV}}$ ground states, but also of satellites, such as r, s, and t, which are predicted to be produced by both processes—collisional inner-shell excitation and dielectronic recombination. We may therefore conclude that the observed satellite features are fully described by these two theoretically considered processes of excitation. On the other hand, we found that the intensity ratios x/w, y/w, and z/w of the heliumlike lines were substantially larger at low electron temperatures than the values expected from electron impact excitation.

Important for an experimental verification of the theory is a comparison of the obtained parameter values of T_e, $n_{\text{Ni XXVI}}/n_{\text{Ni XXVII}}$, and $n_{\text{Ni XXV}}/n_{\text{Ni XXVII}}$ with the results from independent electron-temperature measurements and coronal-equilibrium calculations; and it is also necessary to compare the observed intensity ratios x/w, y/w, and z/w with the more complete theoretical predictions which include the additional processes of excitation mentioned in Sec. I. These detailed comparisons of the theory with the experimental data are given in the following subsections.

A. Electron temperature results

The electron-temperature values, which were derived from the least-squares fits of the Ni XXVII spectra, are shown in Fig. 6, together with the central electron temperature results obtained from the laser Thomson-scattering [26] diagnostic and the x-ray PHA system [27]. The PHA data and the Ni XXVII spectra were accumulated during the entire three-second period of steady-state conditions of each discharge. These data result from chord-averaged measurements. By contrast, the Thomson-scattering diagnostic provides instantaneous and local measurement of the electron temperature. The T_e results from the PHA system have been corrected for profile effects based on the shapes of the radial electron-temperature profiles obtained from the Thomson-scattering diagnostic.

We infer from Fig. 6 that the electron temperature results derived from the Ni XXVII spectra agree with the electron temperature results from the PHA system to within the error bars, and that they are also in good agreement with the Thomson-scattering data. The error for the T_e values obtained from the least-squares-fit analysis of the Ni XXVII spectra is in the range 50 to 120 eV. This error reflects the good agreement between the synthetic and observed spectra, since the statistical errors of the experimental data were small.

B. Ion charge-state distribution

The density ratios $n_{\text{Ni XXVI}}/n_{\text{Ni XXVII}}$ and $n_{\text{Ni XXV}}/n_{\text{Ni XXVII}}$ obtained from the analysis of the satellite spectra are shown in Figs. 7 and 8 as a function of the electron temperature. Also shown are theoretical predictions for coronal equilibrium from Breton *et al.* [7] and Hulse [28] as well as the most recent results from Zastrow, Källne, and Summers [9]. The coronal-equilibrium curves shown

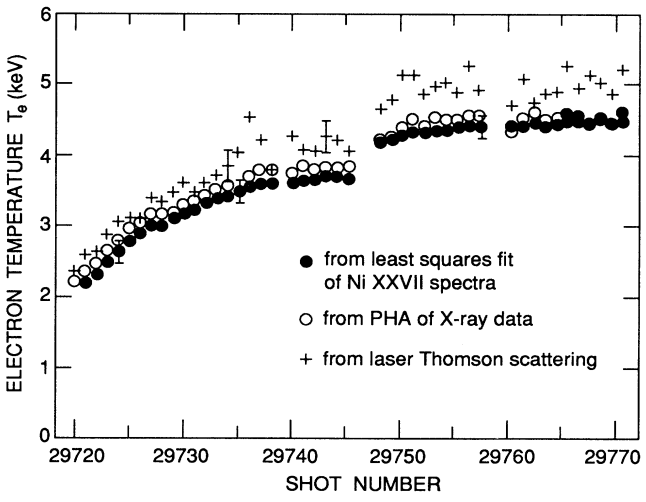

FIG. 6. Comparison of the electron temperature values derived from least-squares fits to the Ni XXVII spectra with the central-electron-temperature data from the Thomson-scattering diagnostic and the PHA system.

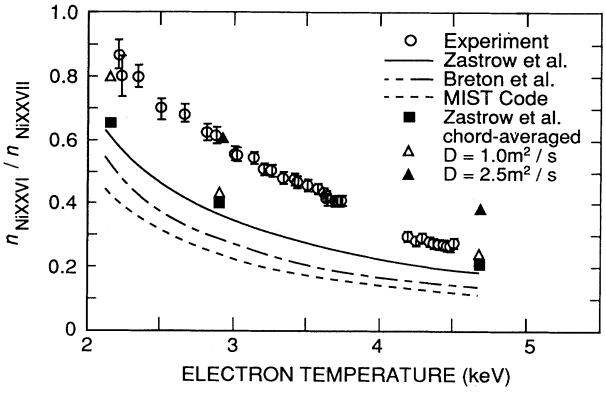

FIG. 7. Relative abundances of lithiumlike and heliumlike nickel as obtained from the analysis of the spectral data, and theoretical predictions from different coronal-equilibrium calculations. The squares represent ratios of the line-averaged abundances corresponding to the coronal-equilibrium predictions by Zastrow, Källne, and Summers (Ref. [9]). (See text). The triangles represent values obtained from MIST-code transport calculations assuming different values for the diffusion constant.

in Figs. 7 and 8 have been calculated under the assumption that radial profile effects are negligible, i.e., these curves represent the coronal-equilibrium values predicted for the central electron temperatures. The observed relative abundances $n_{\mathrm{Ni\,XXVI}}/n_{\mathrm{Ni\,XXVII}}$ and $n_{\mathrm{Ni\,XXV}}/n_{\mathrm{Ni\,XXVII}}$, are significantly larger than these predicted values for the entire range of electron temperatures. As possible explanations for these observed deviations we considered the following.

(1) Charge-exchange recombination of nickel ions with neutral hydrogen, which is not included in the present coronal-equilibrium calculations, is important.

(2) Radial-profile effects are not negligible even though the charge-state distribution is in coronal equilibrium.

(3) Radial ion transport must be included to describe the ion charge-state distribution in tokamak plasmas.

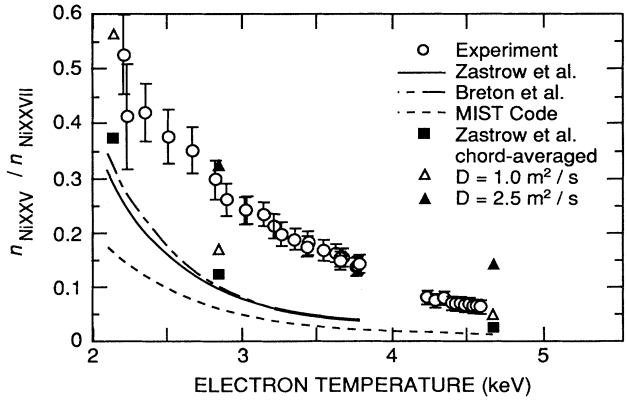

FIG. 8. Relative abundances of berylliumlike and heliumlike nickel from the analysis of the spectral data and theoretical predictions as described in the caption of Fig. 7.

(4) The coronal equilibrium predictions are affected by theoretical uncertainties of the ionization and recombination rate coefficients used in the calculations.

We will show that effects (1) and (2) cannot account for the observed deviations. However, the possibilities (3) and (4) must be considered for interpretation of the experimental data. At the present time, no clear distinction can be made as to which of these last two possibilities is responsible for the observed deviations.

The process of charge-exchange recombination mentioned in (1) was discussed in Ref. [8]. The effects of charge-exchange recombination on the nickel-ion charge-state distribution were estimated not to be significant in the center of the large JET tokamak plasmas with Ohmic heating. This process should be even less important for the helium-prefill TFTR discharges used in the present experiments.

In order to determine the magnitude of radial profile effects mentioned in (2), we assumed that the ion charge-state distribution was in coronal equilibrium as given by Zastrow, Källne, and Summers [9]. We then calculated chord integrals of the line emissivities for the lines w, q, and β, and derived "chord-averaged" values for the abundances of Ni XXVII, Ni XXVI, and Ni XXV, given by

$$\langle n_{\mathrm{Ni\,XXVII}}\rangle = \frac{\int_{R_{\min}}^{R_{\max}} \langle \sigma v\rangle_w \frac{n_{\mathrm{Ni\,XXVII}}}{n_{\mathrm{Ni}}} n_e n_{\mathrm{Ni}} dl}{\int_{R_{\min}}^{R_{\max}} \langle \sigma v\rangle_w n_e dl},$$

$$\langle n_{\mathrm{Ni\,XXVI}}\rangle = \frac{\int_{R_{\min}}^{R_{\max}} \langle \sigma v\rangle_q \frac{n_{\mathrm{Ni\,XXVI}}}{n_{\mathrm{Ni}}} n_e n_{\mathrm{Ni}} dl}{\int_{R_{\min}}^{R_{\max}} \langle \sigma v\rangle_q n_e dl},$$

and

$$\langle n_{\mathrm{Ni\,XXV}}\rangle = \frac{\int_{R_{\min}}^{R_{\max}} \langle \sigma v\rangle_\beta \frac{n_{\mathrm{Ni\,XXV}}}{n_{\mathrm{Ni}}} n_e n_{\mathrm{Ni}} dl}{\int_{R_{\min}}^{R_{\max}} \langle \sigma v\rangle_\beta n_e dl}.$$

Here, $\langle \sigma v\rangle_w$, $\langle \sigma v\rangle_q$, and $\langle \sigma v\rangle_\beta$ are the rate coefficients for electron-impact excitation of the lines w, q, and β taken from Ref. [8]; $n_{\mathrm{Ni\,XXVII}}/n_{\mathrm{Ni}}$, $n_{\mathrm{Ni\,XXVI}}/n_{\mathrm{Ni}}$, and $n_{\mathrm{Ni\,XXVI}}/n_{\mathrm{Ni}}$ are the fractional ion charge-state abundances for coronal equilibrium taken from Ref. [9]; n_e and n_{Ni} are the electron density and the total density of the nickel impurity. We assumed $n_{\mathrm{Ni}} = 0.001 n_e$.

The chord integrals were performed for shots 29 720, 29 726, and 29 766 using the experimentally observed radial profiles of the electron temperature and electron density (see Figs. 1 and 2). Ratios of the obtained *chord-averaged* abundances, $\langle n_{\mathrm{Ni\,XXVI}}\rangle/\langle n_{\mathrm{Ni\,XXVII}}\rangle$ and $\langle n_{\mathrm{Ni\,XXV}}\rangle/\langle n_{\mathrm{Ni\,XXVII}}\rangle$, are shown in Figs. 7 and 8, respectively, by the solid square symbols. The ratios of the chord-averaged abundances are not very different from the ratios $n_{\mathrm{Ni\,XXVI}}/n_{\mathrm{Ni\,XXVII}}$ and $n_{\mathrm{Ni\,XXV}}/n_{\mathrm{Ni\,XXVII}}$ (solid lines) obtained from the theoretical data of Zastrow, Källne, and Summers [9] for the (single) central-electron-temperature values. This justifies the assumption made

in Sec. III, that chord integrals of the line emissivities are not essential for the analysis of the present data.

We note that the chord-averaged abundances introduced above to quantify the deviations from coronal equilibrium are not directly measurable quantities. Following Zastrow, Källne, and Summers [9], we therefore also compared ratios of chord-integrated line emissivities with observed intensity ratios. Figure 9 shows such a comparison for the intensity ratios of the lines q and w: The solid line presents ratios of the emissivities for q and w, evaluated for the central electron temperature and assuming the coronal-equilibrium conditions of Ref. [9]; the triangles represent ratios of chord-integrated emissivities evaluated for shots 29 720, 29 726, and 29 766 from the measured electron density and temperature profiles, again with the assumption of the coronal-equilibrium conditions of Ref. [9].

We infer from Figs. 7–9 that the observed charge-state distribution and the observed intensity ratios are *not* in agreement with theoretical coronal-equilibrium predictions. We note that the intensity of the line q was evaluated by subtracting the contributions for the line y from the observed spectral feature, which is a blending of these two lines. However, the subtracted contribution of the line y was larger than the theoretically predicted values, as discussed in Sec. IV C.

In order to put the analysis of the present TFTR data in perspective with the analysis of the JET data in Ref. [8], we compare in Table I our results from the spectrum shown in Fig. 5(a) with the results obtained by Bombarda *et al.* [8]. We note that the spectrum in Fig. 5(a) is very similar to the spectrum presented in Fig. 6 of Ref. [8]. We infer from Table I that the results from the analysis of the present data are essentially the same as those reported by Bombarda *et al.* [8]. The data given in Table I and the data shown in Figs. 7 and 8 suggest that coronal equilibrium alone does not provide an adequate description of the ionization balance for the highest ionization states of nickel either in JET or TFTR tokamak plasmas.

A detailed inspection of the experimental data shown in Figs. 7 and 8 indicates that radial ion transport mentioned in (3) should be included in order to describe the observed charge-state distributions. We have, therefore, performed plasma-modeling calculations using the one-dimensional multi-ion-species-transport (MIST) code [28]. The MIST code solves a coupled set of continuity equations for each charge state of a given impurity element, taking into account the various processes of ionization and recombination as well as crossfield ion transport. The transport flux is parameterized by a single spatially constant diffusion coefficient D and a convective pinch velocity, which for the present analysis was chosen to produce an equilibrium total-nickel-density profile proportional to the electron-density profile.

The code calculations were performed for the measured electron density and electron temperature profiles from shots 27 920, 27 926, and 27 966 (using ionization and recombination rate coefficients corresponding to those in the most recent calculations of Ref. [9]). From these model calculations we found that the observed abundance ratios can be reproduced with the following values for the diffusion constant D: $D = 1\ \mathrm{m^2\,s^{-1}}$ for shot 29 720, $D = 2.5\ \mathrm{m^2\,s^{-1}}$ for shot 29 726, and $D = 1\ \mathrm{m^2\,s^{-1}}$ for shot 27 966 (see also Figs. 7 and 8). These results are consistent with the general observation that transport effects are less important in discharges with higher density and higher plasma currents. From a detailed inspection of the data shown in Figs. 3, 7, and 8, we find that the deviations from coronal equilibrium increase for the first part of the shot sequence (shot numbers 29 720 to 29 745) for which the electron density decreased continuously. The deviations are smaller for the discharges with shot numbers in the range 29 748 to 29 770. We note that these discharges had both a higher magnetic field and higher plasma current, which resulted in a steplike increase in plasma density (see Fig. 3). The fact that the observed relative abundances $n_{\mathrm{Ni\,XXVI}}/n_{\mathrm{Ni\,XXVII}}$ and $n_{\mathrm{Ni\,XXVI}}/n_{\mathrm{Ni\,XXVII}}$ varied with parameters, such as the

TABLE I. Comparison of the results from the present analysis for the spectrum shown in Fig. 5(a) with the analysis results obtained by Bombarda *et al.* for the spectrum shown in Fig. 6 of Ref. [8].

T_e (keV)	T_i (keV)	$n_{\mathrm{Ni\,XXVI}}/n_{\mathrm{Ni\,XXVII}}$	$n_{\mathrm{Ni\,XXV}}/n_{\mathrm{Ni\,XXVII}}$
2.86[a]	2.17[a]	0.62[a] (0.24[c], 0.30[d], 0.37[e])	0.26[a] (0.05[c], 0.10[d,e])
2.8[b]	2.39[b]	0.7[b] (0.330[f])	0.2[b] (0.090[f])

[a]Results from the present analysis for the spectrum in Fig. 5(a) (TFTR).
[b]Analysis results of Bombarda *et al.* for the spectrum given in Fig. 6 of Ref. [8] (JET).
[c]Coronal-equilibrium predictions from Ref. [28].
[d]Coronal equilibrium predictions from Ref. [7].
[e]Coronal equilibrium predictions from Ref. [9].
[f]Coronal equilibrium predictions from Ref. [8].

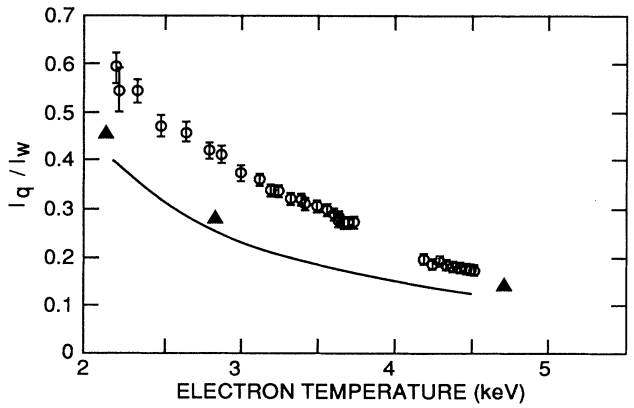

FIG. 9. Comparison of observed intensity ratios for lines q and w (circles) with coronal-equilibrium predictions from Ref. [9] (solid line and triangles). The solid line represents ratios of the line emissivities evaluated for the central electron temperature. The triangles represent ratios of chord-integrated emissivities from measured electron density and temperature profiles for shots 29 720, 29 726, and 29 766.

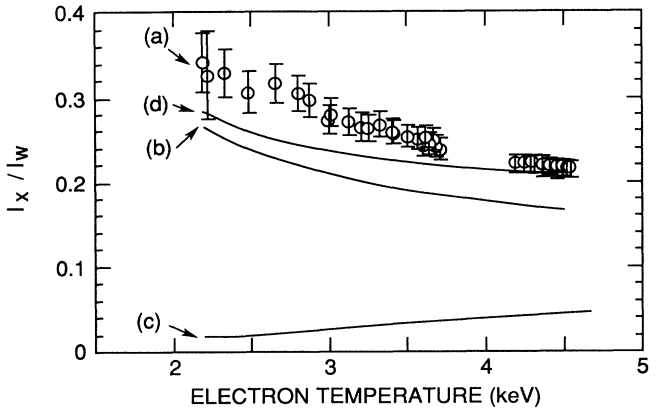

FIG. 10. Intensity ratios of the heliumlike lines x and w as a function of the electron temperature from (a) the analysis of the spectral data and from theoretical predictions for (b) electron impact excitation, (c) excitation by recombination of Ni XXVIII, and (d) total of (b) and (c).

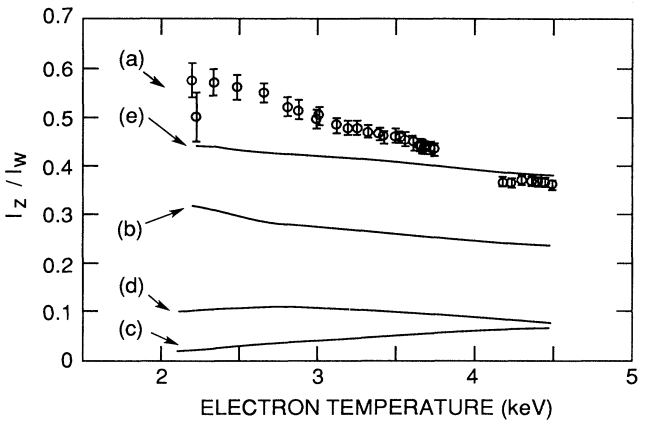

FIG. 12. Intensity ratios of the heliumlike lines z and w as a function of the electron temperature from (a) the analysis of the spectral data and from theoretical predictions for (b) electron impact excitation, (c) excitation by recombination of Ni XXVIII, (d) excitation by inner-shell ionization of Ni XXVI, and (e) total of (b), (c), and (d).

density, plasma current and magnetic field, clearly indicates that the observed abundances were *not* in coronal equilibrium, since coronal equilibrium is *only* a function of the electron temperature.

Transport studies of metal impurities in tokamak plasmas have been performed by a number of authors [29–31] and indicate that the metal-ion charge-state distributions are determined by radial transport as well as atomic processes of ionization and recombination. From an investigation by Stratton *et al.* [31] follows that the values for D in Ohmic TFTR discharges are typically in the range 0.5 to 1.5 $m^2 s^{-1}$. We point out that the results reported on nickel in Ref. [31] were obtained with MIST-code calculations using different ionization and recombination rate coefficients (corresponding to the MIST-code coronal-equilibrium curves shown in Figs. 7 and 8) and for experimental conditions corresponding to those of shots 29 748–29 770. The values for D obtained from the present modeling calculations are of the same order as those reported in Ref. [31]. However, based on the present experiments we cannot exclude that the observed deviations from the coronal equilibrium may also be partially ascribed to the theoretical uncertainties mentioned in (4).

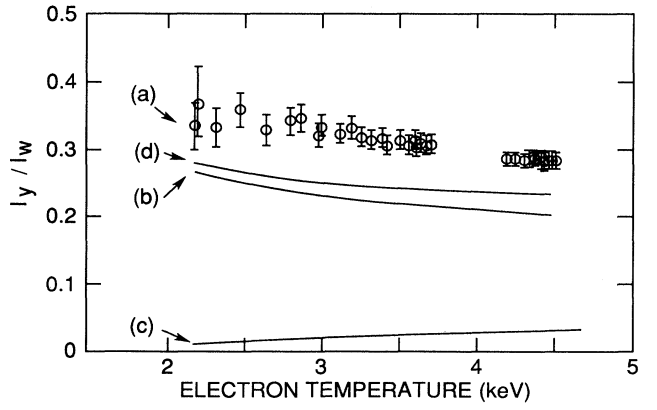

FIG. 11. Intensity ratios of the heliumlike lines y and w as a function of the electron temperature from (a) the analysis of the spectral data and theoretical predictions as in Fig. 10.

C. Intensity ratios of the heliumlike lines

Figures 10–12 show the observed intensity ratios x/w, y/w, and z/w of the heliumlike lines as a function of the electron temperature and, for comparison, the theoretically predicted contributions from different excitation processes: (1) electron impact excitation (including cascades), (2) excitation due to recombination of hydrogenlike nickel, Ni XXVIII, and (3) excitation by inner-shell ionization. The contributions from process (2) were calculated using for the relative abundances of $n_{\mathrm{Ni\,XXVIII}}/n_{\mathrm{Ni\,XXVII}}$ the coronal equilibrium data given by Zastrow, Källne, and Summers [9]. The contribution from process (3) to the intensity ratio z/w is proportional to the density ratio of $n_{\mathrm{Ni\,XXVI}}/n_{\mathrm{Ni\,XXVII}}$. This contribution has been determined using the measured density ratios $n_{\mathrm{Ni\,XXVI}}/n_{\mathrm{Ni\,XXVII}}$ shown in Fig. 7.

We infer from Figs. 10–12 that the observed intensity ratios decrease with increasing electron temperature in a way similar to that of the predicted contributions from process (1). However, this process alone does not account for the observed intensity ratios. Numerical agreement for the line ratios x/w and z/w is obtained for a small range of electron temperatures near 3.5 keV by including the contributions from processes (2) and (3) (see Figs. 10 and 12). Numerical agreement for the line ratio y/w can be fortuitously obtained by increasing the density ratio $n_{\mathrm{Ni\,XXVI}}/n_{\mathrm{Ni\,XXVII}}$. This is due to the fact that the line y is blended with the satellite q,

$1s^2 2s\ ^2S_{1/2} - 1s2s2p\ ^2P_{3/2}$. This satellite is produced by collisional inner-shell excitation, and its intensity is proportional to $n_{\text{Ni XXVI}}/n_{\text{Ni XXVII}}$. The use of the least-squares-fits method in our analysis (step 3 in Sec. III) removes the arbitrariness in determining the parameter $n_{\text{Ni XXVI}}/n_{\text{Ni XXVII}}$, and clearly reveals the existing discrepancies for y/w.

We note that the discrepancies between theory and experiment are largest at low electron temperatures, near 2 keV. For these low electron temperatures, the abundances of hydrogenlike nickel, and thus the contributions ascribed to process (2), are negligible. We conclude that the theoretically considered processes do not describe the observations for the whole range of electron temperatures.

D. Effects of unresolved $n \geq 3$ satellites on Doppler measurements of the resonance line w

Measurements of the Doppler broadening and Doppler shift of the heliumlike resonance line w are important for evaluating the central ion temperature and plasma rotation velocity in tokamak plasmas [32]. Unfortunately, $n \geq 3$ satellites are blended with the resonance line and cause both an increase of the width and a shift of the so-called "apparent" resonance-line profile. These effects are especially important at low electron temperatures.

In order to determine the magnitude of this effect for ion-temperature measurements, we compare in Fig. 13 ion-temperature results obtained from a single-Voigt-function fit to the "apparent" resonance-line profile (ignoring contributions from unresolved satellites) with those obtained from the complete least-squares-fit analysis (see Sec. III). The ion-temperature values obtained from the single-Voigt-function fit are higher than those obtained from the complete analysis. The relative difference of these ion-temperature results is about 20% for electron temperatures near 2 keV and decreases with increasing electron temperature.

The shift of the "apparent" resonance line, which is caused by unresolved satellites, is a function of both the electron and the ion temperatures [12]. The results obtained are shown in Fig. 14. These relative line shifts were determined from the wavelength difference between the "true" and the "apparent" resonance lines in the synthetic spectra. The error bars shown in Fig. 14 result from the least-squares-fit analysis. The unresolved dielectronic satellites produce a red shift of the "apparent" resonance line. The red shifts are of the order of $\Delta\lambda/\lambda = 2\times10^{-5}$ for electron temperatures of 2 to 3 keV. These line shifts must be taken into account as corrections for Doppler shift measurements.

V. CONCLUSIONS

Satellite spectra of the $K\alpha$ line of heliumlike nickel, Ni XXVII, were recorded from a series of Ohmic TFTR discharges with well-defined plasma parameters and compared with theoretical predictions. The analysis was based on the method of least-squares fits of synthetic spectra to the experimental data, in order to determine the relevant parameters with accuracy. It is found that the observed satellite spectra, which consist of more than 100 lines, are well described by only three parameters: the electron temperature T_e, and the relative abundances $n_{\text{Ni XXVI}}/n_{\text{Ni XXVII}}$ and $n_{\text{Ni XXV}}/n_{\text{Ni XXVII}}$. We conclude that the satellite features and their excitation by dielectronic recombination and collisional inner-shell excitation are correctly described by the theory.

The electron temperature results, which were derived from the relative intensity of the *dielectronic* satellites and the resonance line w, are in good agreement with independent electron temperature measurements by the x-ray pulse height analysis system and the Thomson scattering diagnostics. However, the inferred relative

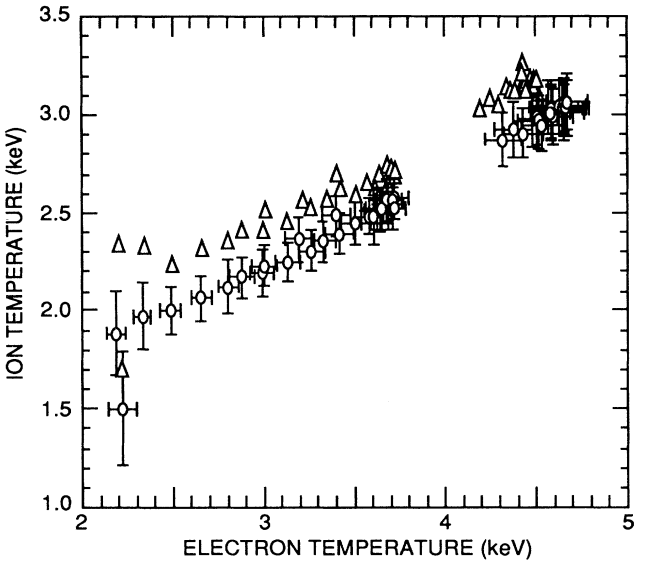

FIG. 13. Ion-temperature results derived from the "apparent" profile of the resonance line w by least-squares fits of single Voigt functions (triangles) and from a complete analysis (circles) as described in Sec. III.

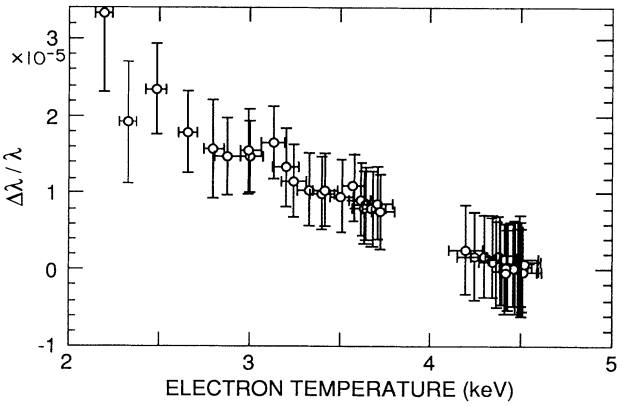

FIG. 14. Red shift of the "apparent" resonance-line profile due to unresolved $n \geq 3$ satellites as a function of the electron temperature.

abundances $n_{\text{Ni XXVI}}/n_{\text{Ni XXVII}}$ and $n_{\text{Ni XXV}}/n_{\text{Ni XXVII}}$ are systematically higher than the coronal-equilibrium predictions for the entire investigated range of electron temperatures, 2–5 keV. The deviations from coronal-equilibrium predictions can be explained by radial ion transport with (spatially constant) ion diffusion coefficients in the range $1-2.5\ \text{m}^2\text{s}^{-1}$. To some extent, the deviations may be ascribed to the theoretical uncertainties of the ionization and recombination rate coefficients used for the coronal-equilibrium calculations.

Systematic discrepancies are found between the predicted and the observed relative intensities of the helium-like lines w, x, y, and z.

The broadening and shift of the "apparent" resonance-line profile, which is produced by unresolved dielectronic $n \geq 3$ satellites, has been determined as a function of the electron temperature. These effects must be taken into account for measurements of the ion temperature and the plasma rotation in tokamak plasmas.

ACKNOWLEDGMENTS

We are grateful to K.-D. Zastrow, E. Källne, and H. P. Summers for making their recent coronal equilibrium data available to us and for their comments. We appreciate the expert help of N. Schechtman in developing software for the data analysis. We gratefully acknowledge the continuing support of D. M. Meade and K. M. Young, and the technical assistance of J. Gorman and R. Such, and the TFTR operating crew. This work was supported by the U.S. Department of Energy, Contract No. DE-AC02-76-CH0-3073. One of us (L.A.K.) gratefully acknowledges the support by the New Jersey Teachers Research program.

*Permanent address: Laboratoire de Physique Atomique et Nucléaire, Université Pierre et Marie Curie, F-75231 Paris, CEDEX 05, France.

†Permanent address: Princeton High School, 151 Moore Street, Princeton, NJ 08540.

[1] H. Hsuan, M. Bitter, K. W. Hill, S. von Goeler, B. Grek, D. Johnson, L. C. Johnson, S. Sesnic, C. P. Bhalla, K. R. Karim, F. Bely-Dubau, and P. Faucher, Phys. Rev. A **35**, 4280 (1987).

[2] C. P. Bhalla and K. R. Karim, Phys. Rev. A **34**, 3525 (1986).

[3] K. R. Karim and C. P. Bhalla, Phys. Rev. A **34**, 4743 (1986).

[4] U. I. Safronova, J. Quant. Spectrosc. Radiat. Transfer **15**, 231 (1975).

[5] U. I. Safronova, A. m. Urnov, and L. A. Vainshtein, Proc. P. N. Lebedev Phys. Inst. [Acad. Sci. USSR] **119**, 13 (1980).

[6] A. H. Gabriel, Mon. Not. R. Astron. Soc. **160**, 99 (1972).

[7] C. Breton, C. De Michelis, M. Finkenthal, and M. Matioli, Fontenay-aux-Roses Laboratory Report No. EUR-CEA-FC-948, 1978 (unpublished).

[8] F. Bombarda, R. Giannella, E. Källne, G. J. Tallents, F. Bely-Dubau, P. Faucher, M. Cornille, J. Dubau, and A. H. Gabriel, Phys. Rev. A **37**, 504 (1988).

[9] K.-D. Zastrow, E. Källne, and H. P. Summers, Phys. Rev. A **41**, 1427 (1990).

[10] J. Dubau, M. Loulergue, and L. Steenman-Clark, Mon. Not. R. Astron. Soc. **190**, 125 (1980).

[11] J. Dubau, A. H. Gabriel, M. Loulergue, L. Steenman-Clark, and S. Volonte, Mon. Not. R. Astron. Soc. **191**, 705 (1981).

[12] M. Bitter, K. W. Hill, M. Zarnstorff, S. von Goeler, R. Hulse, L. C. Johnson, N. R. Sauthoff, S. Sesnic, K. M. Young, M. Tavernier, F. Bely-Dubau, P. Faucher, M. Cornille, and J. Dubau, Phys. Rev. A **32**, 3011 (1985).

[13] R. W. P. McWhirther, in *Course on Plasma Diagnostics and Data Acquisition Systems, Varenna–Villa Monastero–Italy, September 3–11, 1975,* edited by H. Eubank and E. Sindoni (Editrice Compositori, Bologna, 1975).

[14] G. A. Linford and C. J. Wolfson, Astrophys. J. **331**, 1036 (1988).

[15] D. L. McKenzie, Astrophys. J. **322**, 512 (1987).

[16] P. Lee, A. J. Lieber, A. K. Pradhan, and Yeuming Xu, Phys. Rev. A **34**, 3210 (1986).

[17] R. Bartiromo, F. Bombarda, and R. Giannella, Phys. Rev. A **32**, 531 (1985).

[18] A. K. Pradhan, and J. Michael Shull, Astrophys. J. **249**, 821 (1981).

[19] A. H. Gabriel, and C. Jordan, Mon. Not. R. Astron. Soc. **145**, 705 (1969).

[20] A. H. Gabriel, and C. Jordan, in *Case Studies in Atomic Collisions Physics–II,* edited by McDaniel and McDowell (North-Holland, Amsterdam, 1972).

[21] R. Mewe and J. Schrijver, Astron. Astrophys. **65**, 99 (1978).

[22] R. Mewe and J. Schrijver, Astron. Astrophys. Suppl. **33**, 311 (1978).

[23] R. Mewe and J. Schrijver, Astron. Astrphys. **87**, 55 (1980).

[24] L. A. Vainshtein and U. I. Safronova, P. N. Lebedev Physical Insitute, Moscow, Institute of Spectroscopy, Troizk, and U.S.S.R. Academy of Science, Moscow, U.S.S.R. Rep. 3 (unpublished).

[25] H. Hsuan, M. Bitter, J. E. Rice, K. W. Hill, L. Johnson, S. L. Liew, S. D. Scott, and S. von Goeler, Rev. Sci. Instrum. **59**, 2127 (1988).

[26] D. Johnson, D. Dimock, B. Grek, D. Long, D. McNeill, R. Palladino, J. Robinson, and E. Tolnas, Rev. Sci. Instrum. **56**, 1015 (1985).

[27] K. W. Hill, M. Bitter, M. Diesso, L. Dudek, S. von Goeler, S. Hayes, L. C. Johnson, J. Kiraly, E. Moshey, G. Renda, S. Sesnic, N. R. Sauthoff, F. Tenney, and K. M. Young, Rev. Sci. Instrum. **56**, 840 (1985).

[28] R. A. Hulse, Nucl. Technol. Fusion **3**, 259 (1983).

[29] K. D. Behringer, P. G. Carolan, B. Denne, *et al.,* Nucl. Fusion **26**, 751 (1986).

[30] E. S. Marmar, J. E. Rice, J. L. Terry, and F. H. Seguin, Nucl. Fusion **22**, 1567 (1982).

[31] B. C. Stratton, R. J. Fonck, R. A. Hulse, A. T. Ramsey, J. Timberlake, P. C. Efthimion, E. D. Fredrickson, B. Grek, K. W. Hill, D. J. Johnson, D. K. Mansfield, H. Park, F. J. Stauffer, and G. Taylor, Nucl. Fusion **29**, 437 (1986).

[32] TFTR Group, M. Bitter *et al.,* Plasma Phys. Controlled Fusion **29**, 1235 (1987).